

Update of Short-Baseline Electron Neutrino and Antineutrino Disappearance

C. Giunti

INFN, Sezione di Torino, Via P. Giuria 1, I-10125 Torino, Italy

M. Laveder

*Dipartimento di Fisica e Astronomia “G. Galilei”, Università di Padova,
and INFN, Sezione di Padova, Via F. Marzolo 8, I-35131 Padova, Italy*

Y.F. Li

Institute of High Energy Physics, Chinese Academy of Sciences, Beijing 100049, China

Q.Y. Liu, H.W. Long

Department of Modern Physics, University of Science and Technology of China, Hefei, Anhui 230026, China

We present a complete update of the analysis of ν_e and $\bar{\nu}_e$ disappearance experiments in terms of neutrino oscillations in the framework of 3+1 neutrino mixing, taking into account the Gallium anomaly, the reactor anomaly, solar neutrino data and $\nu_e C$ scattering data. We discuss the implications of a recent ${}^{71}\text{Ga}({}^3\text{He}, {}^3\text{H}){}^{71}\text{Ge}$ measurement which give information on the neutrino cross section in Gallium experiments. We discuss the solar bound on active-sterile mixing and present our numerical results. We discuss the connection between the results of the fit of neutrino oscillation data and the heavy neutrino mass effects in β -decay experiments (considering new Mainz data) and neutrinoless double- β decay experiments (considering the recent EXO results).

PACS numbers: 14.60.Pq, 14.60.Lm, 14.60.St

I. INTRODUCTION

In recent years several short-baseline neutrino oscillation experiments have found anomalies which may require an extension of the standard three-neutrino mixing framework which describes the neutrino oscillations observed in solar, atmospheric and long-baseline experiments (see [1–3]). In this paper we consider the Gallium anomaly [4–6] and the reactor anomaly [7–9], which indicate that electron neutrino and antineutrinos may disappear at short distances¹. Such disappearance may be explained by the presence of at least one massive neutrino at the eV scale, which drives short-baseline neutrino oscillations generated by a squared-mass difference which is much larger than the squared-mass difference operating in the solar, atmospheric and long-baseline neutrino oscillation experiments. We consider 3+1 neutrino mixing, which is the minimal extension of three-neutrino mixing which can explain the Gallium and reactor anomalies. Since from the LEP measurement of the invisible width of the Z boson [13] we know that there are only three light active flavor neutrinos the additional neutrino in the 3+1 framework is sterile.

In this paper we discuss the implications of the recent ${}^{71}\text{Ga}({}^3\text{He}, {}^3\text{H}){}^{71}\text{Ge}$ measurement in Ref. [14], which give information on the neutrino cross section in Gallium experiments. We take also into account the most updated

calculation of the reactor neutrino fluxes presented in the recent White Paper on light sterile neutrinos [15]. We present also a detailed discussion of the connection between the results of the fit of neutrino oscillation data and the results of β -decay experiments (considering the Mainz data presented very recently in Ref. [16]) and neutrinoless double- β decay experiments (considering the recent EXO bound in Ref. [17] and the controversial positive result in Ref. [18]).

We consider 3+1 neutrino mixing as an extension of standard three-neutrino mixing. The mixing of the three active flavor neutrino fields ν_e , ν_μ , ν_τ and one sterile neutrino field ν_s is given by

$$\nu_\alpha = \sum_{k=1}^4 U_{\alpha k} \nu_k, \quad (1)$$

where U is the unitary 4×4 mixing matrix ($U^\dagger = U^{-1}$) and each of the four ν_k 's is a massive neutrino field with mass m_k . We consider the squared-mass hierarchy

$$\Delta m_{21}^2 \ll \Delta m_{31}^2 \ll \Delta m_{41}^2, \quad (2)$$

with $\Delta m_{kj}^2 \equiv m_k^2 - m_j^2$, such that Δm_{21}^2 generates the very-long-baseline oscillations observed in solar neutrino experiments and in the KamLAND reactor antineutrino experiment, Δm_{31}^2 generates the long-baseline oscillations observed in atmospheric neutrino experiments and in long-baseline accelerator and reactor neutrino and antineutrino experiments, and Δm_{41}^2 generates short-baseline oscillations.

The effective survival probability at a distance L of electron neutrinos and antineutrinos with energy E in

¹ The inclusion in the analysis of the more controversial LSND [10] and MiniBooNE [11] $\bar{\nu}_\mu \rightarrow \bar{\nu}_e$ anomalies will be discussed elsewhere [12].

short-baseline neutrino oscillation experiments is given by (see Refs. [19–22])

$$P_{\nu_e \rightarrow \nu_e}^{\text{SBL}(-)} = 1 - \sin^2 2\vartheta_{ee} \sin^2 \left(\frac{\Delta m_{41}^2 L}{4E} \right), \quad (3)$$

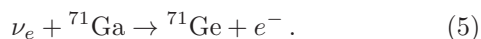
with the transition amplitude

$$\sin^2 2\vartheta_{ee} = 4|U_{e4}|^2 (1 - |U_{e4}|^2). \quad (4)$$

The plan of the paper is as follows. In Section II we discuss in detail the Gallium ν_e anomaly [4–6] and the implications of the important recent $^{71}\text{Ga}(^3\text{He}, ^3\text{H})^{71}\text{Ge}$ measurement in Ref. [14]. In Section III we present the results of the combined analysis of Gallium data with reactor $\bar{\nu}_e$ data, taking into account the reactor $\bar{\nu}_e$ anomaly [7–9, 15]. In Section IV we discuss the solar neutrino constraint on short-baseline ν_e disappearance [23–26]. In Section V we present the results of the global fit of ν_e and $\bar{\nu}_e$ disappearance data, which includes also $\nu_e + ^{12}\text{C} \rightarrow ^{12}\text{N}_{\text{g.s.}} + e^-$ scattering data [27, 28]. We confront these results with the bounds on the heavy neutrino mass given by the data of β -decay experiments [16, 29] and neutrinoless double- β decay experiments [17, 18]. Finally, in Section VI we draw our conclusions.

II. GALLIUM ANOMALY

The GALLEX [30–32] and SAGE [33–36] Gallium solar neutrino experiments have been tested with intense artificial ^{51}Cr and ^{37}Ar radioactive sources which produce electron neutrinos through electron capture with the energies and branching ratios given in Tab. I. In each of these experiments the source was placed near the center of the approximately cylindrical detector and electron neutrinos have been detected with the solar neutrino detection reaction



The average neutrino travelling distances are $\langle L \rangle_{\text{GALLEX}} = 1.9\text{ m}$ and $\langle L \rangle_{\text{SAGE}} = 0.6\text{ m}$. The first line in Tab. II shows the ratios R_B of measured and expected ^{71}Ge event rates reported by the experimental collaborations. The index B indicates that the expected event rates have been calculated using the Bahcall cross sections [37]

$$\sigma_B(^{51}\text{Cr}) = 58.1 \times 10^{-46} \text{ cm}^2, \quad (6)$$

$$\sigma_B(^{37}\text{Ar}) = 70.0 \times 10^{-46} \text{ cm}^2, \quad (7)$$

TABLE I. Energy (E) and branching ratio (B.R.) of the neutrino lines produced in the electron-capture decay of ^{51}Cr and ^{37}Ar .

E [keV]	^{51}Cr				^{37}Ar	
	747	752	427	432	811	813
B.R.	0.8163	0.0849	0.0895	0.0093	0.902	0.098

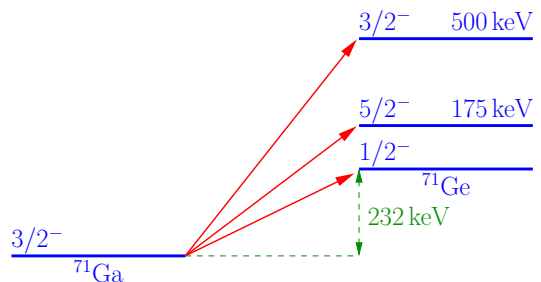


FIG. 1. $^{71}\text{Ga} \rightarrow ^{71}\text{Ge}$ transitions induced by ^{51}Cr and ^{37}Ar electron neutrinos.

without considering their uncertainties. One can see that the values of R_B^{G1} and R_B^{S1} indicate a compatibility between the measured and expected event rates, whereas the values of R_B^{G2} and R_B^{S2} are significantly smaller than one, indicating a disappearance of electron neutrinos. The weighted average in Tab. II gives a 2.7σ anomaly.

Since the values of the cross sections of ^{51}Cr and ^{37}Ar electron neutrinos and their uncertainties are crucial for the interpretation of the Gallium data as indication of short-baseline ν_e disappearance, in the following we discuss in detail the problem of the determination of the cross sections and their uncertainties, taking into account Refs. [37–40] and the important recent measurement in Ref. [14].

The cross sections of the interaction process (5) for neutrinos produced by ^{51}Cr and ^{37}Ar sources are given by

$$\sigma = \sigma_{\text{gs}} \left(1 + \xi_{175} \frac{\text{BGT}_{175}}{\text{BGT}_{\text{gs}}} + \xi_{500} \frac{\text{BGT}_{500}}{\text{BGT}_{\text{gs}}} \right), \quad (8)$$

where σ_{gs} is the cross sections of the transitions from the ground state of ^{71}Ga to the ground state of ^{71}Ge , BGT_{gs} is the corresponding Gamow-Teller strength, and BGT_{175} and BGT_{500} are the Gamow-Teller strengths of the transitions from the ground state of ^{71}Ga to the two excited states of ^{71}Ge at about 175 keV and 500 keV (see Fig. 1). The coefficients of $\text{BGT}_{175}/\text{BGT}_{\text{gs}}$ and $\text{BGT}_{500}/\text{BGT}_{\text{gs}}$ are determined by phase space: $\xi_{175}(^{51}\text{Cr}) = 0.669$, $\xi_{500}(^{51}\text{Cr}) = 0.220$, $\xi_{175}(^{37}\text{Ar}) = 0.695$, $\xi_{500}(^{37}\text{Ar}) = 0.263$ [37].

TABLE II. Ratios of measured and expected ^{71}Ge event rates in the four radioactive source experiments. G1 and G2 denote the two GALLEX experiments with ^{51}Cr sources [30–32], S1 denotes the SAGE experiment with a ^{51}Cr source, and S2 denotes the SAGE experiment with a ^{37}Ar source [33–36]. AVE denotes the weighted average.

	G1	G2	S1	S2	AVE
R_B	$0.95^{+0.11}_{-0.11}$	$0.81^{+0.10}_{-0.11}$	$0.95^{+0.12}_{-0.12}$	$0.79^{+0.08}_{-0.08}$	$0.86^{+0.05}_{-0.05}$
R_{HK}	$0.85^{+0.12}_{-0.12}$	$0.71^{+0.11}_{-0.11}$	$0.84^{+0.13}_{-0.12}$	$0.71^{+0.09}_{-0.09}$	$0.77^{+0.08}_{-0.08}$
R_{FF}	$0.93^{+0.11}_{-0.11}$	$0.79^{+0.10}_{-0.11}$	$0.93^{+0.11}_{-0.12}$	$0.77^{+0.09}_{-0.07}$	$0.84^{+0.05}_{-0.05}$
R_{HF}	$0.83^{+0.13}_{-0.11}$	$0.71^{+0.11}_{-0.11}$	$0.83^{+0.13}_{-0.12}$	$0.69^{+0.10}_{-0.09}$	$0.75^{+0.09}_{-0.07}$

The cross sections of the transitions from the ground state of ^{71}Ga to the ground state of ^{71}Ge have been calculated accurately by Bahcall [37]:

$$\sigma_{\text{gs}}(^{51}\text{Cr}) = 55.3 \times 10^{-46} \text{ cm}^2, \quad (9)$$

$$\sigma_{\text{gs}}(^{37}\text{Ar}) = 66.2 \times 10^{-46} \text{ cm}^2. \quad (10)$$

These cross sections are proportional to the characteristic neutrino absorption cross section [37, 41]

$$\begin{aligned} \sigma_0 &= 2\alpha Z_{\text{Ge}} m_e^2 G_{\text{F}}^2 |V_{ud}|^2 g_A^2 \text{BGT}_{\text{gs}} \\ &= Z_{\text{Ge}} \text{BGT}_{\text{gs}} (3.091 \pm 0.012) \times 10^{-46} \text{ cm}^2, \end{aligned} \quad (11)$$

where α is the fine-structure constant, $Z_{\text{Ge}} = 32$ is the atomic number of the final nucleus, m_e is the electron mass, G_{F} is the Fermi constant, V_{ud} is the ud element of the quark mixing matrix V , and g_A is the axial coupling constant. The numerical value of the coefficient in the last line of Eq. (11) has been obtained with the values of these quantities given in the last Review of Particle Physics [42]. From the value

$$\sigma_0 = (8.611 \pm 0.011) \times 10^{-46} \text{ cm}^2, \quad (12)$$

calculated by Bahcall [37] using the accurate measurement [43]

$$T_{1/2}(^{71}\text{Ge}) = 11.43 \pm 0.03 \text{ d} \quad (13)$$

of the lifetime of ^{71}Ge (which decays through the electron-capture process $e^- + {}^{71}_{32}\text{Ge} \rightarrow {}^{71}_{31}\text{Ga} + \nu_e$, which is the inverse of the ν_e detection process (5)), we obtain

$$\text{BGT}_{\text{gs}} = 0.0871 \pm 0.0004. \quad (14)$$

This value agrees with that given in Ref. [40], but it is different from that recommended in Ref. [14]. Hence, we checked it using the relation

$$\begin{aligned} \text{BGT}_{\text{gs}} &= \frac{[2J_{\text{Ge}} + 1]}{[2J_{\text{Ga}} + 1]} \frac{2\pi^3 \ln 2}{G_{\text{F}}^2 |V_{ud}|^2 m_e^5 g_A^2 ft_{1/2}(^{71}\text{Ge})} \\ &= \frac{6289 \pm 3 \text{ s}}{2g_A^2 ft_{1/2}(^{71}\text{Ge})}, \end{aligned} \quad (15)$$

with $J_{\text{Ge}} = 1/2$ and $J_{\text{Ga}} = 3/2$, and the value

$$\log ft_{1/2}(^{71}\text{Ge}) = 4.3493 \pm 0.0015, \quad (16)$$

obtained with the LOGFT calculator [44] of the National Nuclear Data Center using the lifetime (13). The result,

$$\text{BGT}_{\text{gs}} = 0.0872 \pm 0.0005, \quad (17)$$

is in agreement with the value (14), which will be used in the following.

The Gamow-Teller strengths BGT_{175} and BGT_{500} have been measured in 1985 in the (p, n) experiment of Krofcheck et al. [38, 39] and recently, in 2011, in the $(^3\text{He}, ^3\text{H})$ experiment of Frekers et al. [14]. The results

are listed in Tab. III together with the 1998 shell-model calculation of BGT_{175} of Haxton [40].

The Bahcall cross sections (6) and (7) have been obtained using for BGT_{500} the Krofcheck et al. measurement and for BGT_{175} half of the Krofcheck et al. upper limit [37].

In previous publications [6, 28, 45–48] we used the Haxton shell-model value of BGT_{175} and the (p, n) measured value of BGT_{500} . Although the uncertainties of the Haxton shell-model value of BGT_{175} are so large that BGT_{175} may be negligibly small, the central value is much larger than the upper limit obtained in the (p, n) experiment. According to Ref. [40], this is due to a suppression of the (p, n) value caused by a destructive interference between the spin ($\Delta J = 1, \Delta L = 0$) matrix element and an additional spin-tensor ($\Delta J = 1, \Delta L = 2$) matrix element which operates only in (p, n) transitions. We do not know if the same suppression is operating also in $(^3\text{He}, ^3\text{H})$, which could be the explanation of the smallness of the value of BGT_{175} measured by Frekers et al., which is compatible with the (p, n) upper bound. Moreover, the value of BGT_{500} measured by Frekers et al. has a 2.7σ discrepancy with that measured by Krofcheck et al. Since we cannot solve these problems, we consider the following three approaches which give the cross sections in Tab. IV and the ratios of measured and expected ^{71}Ge event rates in Tab. II:

HK: Haxton BGT_{175} value and Krofcheck et al. BGT_{500} value. This is our old approach adopted in previous publications [6, 28, 45–48]. The cross sections are significantly larger than the Bahcall cross sections in Eqs. (6) and (7), albeit with large uncertainties which make them compatible at the 1σ level.

FF: Frekers et al. values of both BGT_{175} and BGT_{500} . This is a new approach which is motivated by the new $(^3\text{He}, ^3\text{H})$ measurements [14]. The cross sections are only slightly larger than the Bahcall cross sections in Eqs. (6) and (7), mainly because of the larger BGT_{500} .

HF: Haxton BGT_{175} value and Frekers et al. BGT_{500} value. This is a new approach which is motivated by the possibility that the BGT_{175} measured by Frekers et al. suffers of destructive interference between the spin and spin-tensor matrix element and its value is different from the BGT_{175} in Gallium neutrino detection, as discussed by Haxton for the (p, n) experiment [40]. This approach gives the largest cross sections, which however are still compatible with the Bahcall cross sections at the 1σ level.

From the weighted averages of measured and expected ^{71}Ge event rates in Tab. II it follows that the statistical significance of the Gallium anomaly in the three cases is, respectively, about 3.0σ , 2.9σ and 3.1σ . Hence, the new $(^3\text{He}, ^3\text{H})$ cross section measurement of Frekers et

TABLE III. Values of the Gamow-Teller strengths of the transitions from the ground state of ^{71}Ga to the two excited states of ^{71}Ge at 175 keV and 500 keV and their relative values with respect to the Gamow-Teller strength of the transitions to the ground state of ^{71}Ge , given in Eq. (14).

Reference	Method	BGT_{175}	$\frac{\text{BGT}_{175}}{\text{BGT}_{\text{gs}}}$	BGT_{500}	$\frac{\text{BGT}_{500}}{\text{BGT}_{\text{gs}}}$
Krofcheck et al. [38, 39]	$^{71}\text{Ga}(p, n)^{71}\text{Ge}$	< 0.005	< 0.057	0.011 ± 0.002	0.126 ± 0.023
Haxton [40]	Shell Model	0.017 ± 0.015	0.19 ± 0.18		
Frekers et al. [14]	$^{71}\text{Ga}(^3\text{He}, ^3\text{H})^{71}\text{Ge}$	0.0034 ± 0.0026	0.039 ± 0.030	0.0176 ± 0.0014	0.202 ± 0.016

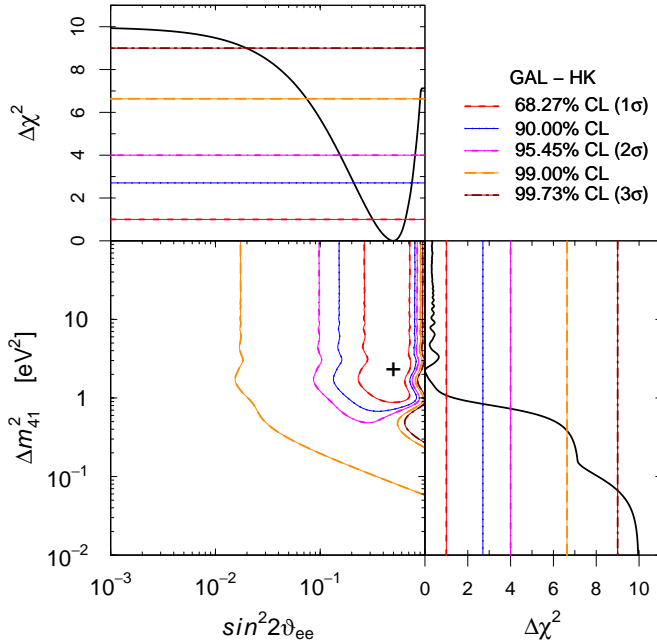


FIG. 2. Allowed regions in the $\sin^2 2\vartheta_{ee} - \Delta m_{41}^2$ plane and marginal $\Delta\chi^2$'s for $\sin^2 2\vartheta_{ee}$ and Δm_{41}^2 obtained from the combined fit of the results of the Gallium radioactive source experiments in the HK case (see the text). The best-fit point corresponding to χ_{\min}^2 is indicated by a cross.

al. [14] confirm that there is a Gallium anomaly at a level of about 3σ [6], which indicates a short-baseline disappearance of ν_e which can be explained by neutrino oscillations.

We analyzed the Gallium data in the three cases above in terms of neutrino oscillations in the 3+1 framework,

TABLE IV. Gallium cross section (in units of 10^{-46} cm^2) and its ratio with the corresponding Bahcall cross section (Eqs. (6) and (7)) for ^{51}Cr and ^{37}Ar neutrinos in the three cases discussed in the text.

	^{51}Cr		^{37}Ar	
	σ	σ/σ_B	σ	σ/σ_B
HK	63.9 ± 6.5	1.10 ± 0.11	77.2 ± 8.1	1.10 ± 0.12
FF	59.2 ± 1.1	1.02 ± 0.02	71.5 ± 1.4	1.02 ± 0.02
HF	64.9 ± 6.5	1.12 ± 0.11	78.5 ± 8.1	1.12 ± 0.12

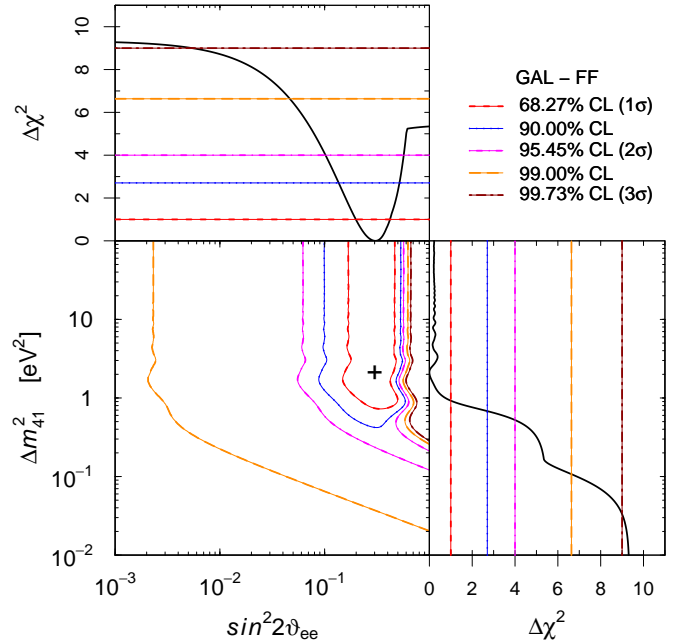


FIG. 3. Allowed regions and marginal $\Delta\chi^2$'s analogous to those in Fig. 2 for the FF case.

in which the effective probability of ν_e survival is given by Eq. (3) with $\alpha = e$. We used the statistical method discussed in Ref. [6], neglecting for simplicity the small difference between the ^{51}Cr and ^{37}Ar cross section ratios in Tab. IV. The results of the fits are presented in Tab. V and Figs. 2–4. One can see that in any case neutrino oscillations give an acceptable fit of the data. In the FF case the goodness-of-fit is smaller than in the HK and HF cases, because of the much smaller uncertainty of

TABLE V. Values of χ^2 , goodness-of-fit (GoF) for 2 degrees of freedom and best-fit values of the 3+1 oscillation parameters obtained from the three fits of Gallium data described in the text.

	HK	FF	HF
χ_{\min}^2	4.8	7.9	4.6
GoF	9.1%	1.9%	9.9%
$\Delta m_{41}^2 [\text{eV}^2]$	2.24	2.1	2.24
$\sin^2 2\vartheta_{ee}$	0.50	0.30	0.52

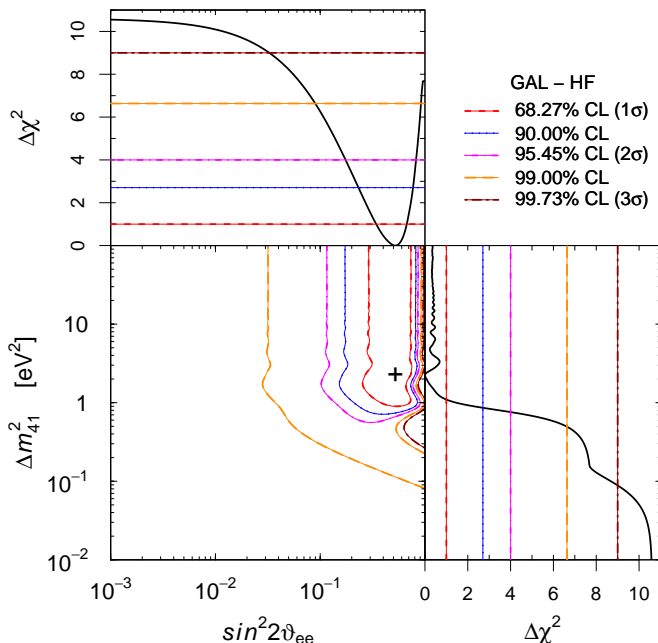


FIG. 4. Allowed regions and marginal $\Delta\chi^2$'s analogous to those in Fig. 2 for the HF case.

BGT₁₇₅. The three cases give approximately the same best-fit value and allowed range of Δm_{41}^2 . Instead, they differ in the best-fit value and allowed range of $\sin^2 2\vartheta_{ee}$: the FF case is in favor of smaller values of $\sin^2 2\vartheta_{ee}$ than the HK and HF cases.

III. FIT OF GALLIUM AND REACTOR DATA

The reactor antineutrino anomaly [9] stems from a new evaluation of the reactor $\bar{\nu}_e$ flux [7, 8] which implies that the event rate measured by several reactor $\bar{\nu}_e$ experiments at distances from the reactor core between about 10 and 100 meters is smaller than that obtained without $\bar{\nu}_e$ disappearance. This is illustrated in Fig. 5, where we plotted the ratio R of the observed $\bar{\nu}_e$ event rate and that expected in absence of $\bar{\nu}_e$ disappearance for the Bugey-3 [49], Bugey-4 [50], ROVNO91 [51], Gosgen [52], ILL [53] and Krasnoyarsk [54] reactor antineutrino experiments. We used the reactor neutrino fluxes presented in the recent White Paper on light sterile neutrinos [15], which updates Refs. [7–9]. From Fig. 5 one can see that the reactor antineutrino anomaly has a significance of about 2.8σ . In the fit of reactor data, besides the above-mentioned rates, we consider also the 40 m/15 m spectral ratio measured in the Bugey-3 experiment [49].

The results of the fit of the reactor antineutrino data are presented in Tab. VI and Fig. 6. One can see that the preferred range of Δm_{41} has a large overlap with that indicated by the Gallium anomaly, but there is a strong upper bound for $\sin^2 2\vartheta_{ee}$ of about 0.3. Therefore, the large- $\sin^2 2\vartheta_{ee}$ part of the Gallium-allowed region in each

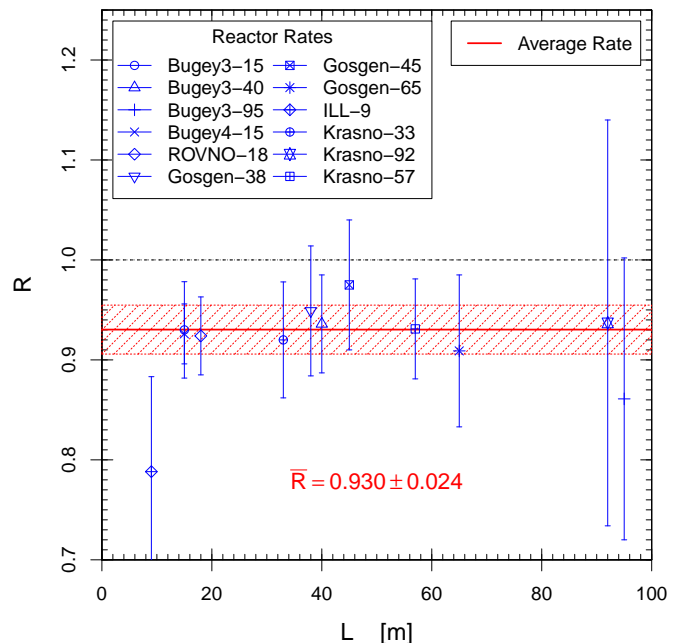


FIG. 5. Ratio R of the observed $\bar{\nu}_e$ event rate and that expected in absence of $\bar{\nu}_e$ disappearance in reactor neutrino experiments. The horizontal band represents the average value of R with 1σ uncertainties.

of the three cases considered in Figs. 2–4 is excluded by reactor data.

The results of the combined fit of Gallium and reactor data are presented in Tab. VI and Figs. 7–9. From these figures, one can see that the allowed regions in the $\sin^2 2\vartheta_{ee}$ – Δm_{41}^2 in the three cases that we have considered for the fit of Gallium data are quite similar, and the best-fit values of $\sin^2 2\vartheta_{ee}$ and Δm_{41}^2 are equal (see Tab. VI). This is due to a dominance of reactor data, which are more numerous and have smaller uncertainties. Hence, in the following we consider only the FF case,

TABLE VI. Values of χ^2 , number of degrees of freedom (NDF), goodness-of-fit (GoF) and best-fit values of the 3+1 oscillation parameters obtained from the fit of reactor (REA) antineutrino data (first column) and from the combined fit of reactor and Gallium data in the three cases discussed in Section II. The last three lines give the parameter goodness-of-fit (PG) [55] of the combined fit.

	REA	REA+HK	REA+FF	REA+HF
χ_{\min}^2	21.5	30.6	31.8	31.0
NDF	36	40	40	40
GoF	97%	86%	82%	85%
Δm_{41}^2 [eV ²]	1.9	1.95	1.95	1.95
$\sin^2 2\vartheta_{ee}$	0.13	0.16	0.16	0.16
$\Delta\chi_{\text{PG}}^2$		4.3	2.4	4.8
NDF _{PG}		2	2	2
GoF _{PG}		12%	30%	9%

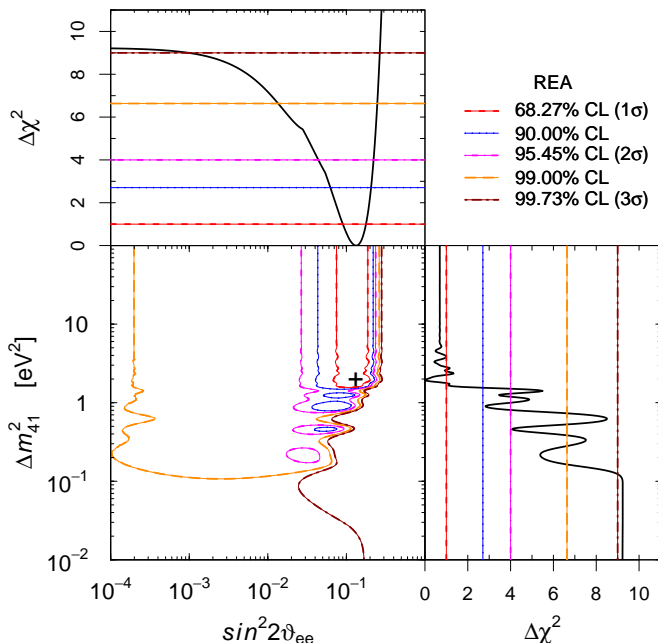


FIG. 6. Allowed regions in the $\sin^2 2\theta_{ee}-\Delta m_{41}^2$ plane and marginal $\Delta\chi^2$'s for $\sin^2 2\theta_{ee}$ and Δm_{41}^2 obtained from the combined fit of reactor antineutrino data. The best-fit point corresponding to χ_{\min}^2 is indicated by a cross.

which is the one which is more compatible with reactor data, because it agrees more than the HK and HF cases with the reactor exclusion of large values of $\sin^2 2\theta_{ee}$. This better agreement is quantified by the larger parameter goodness-of-fit [55] in Tab. VI.

IV. SOLAR NEUTRINO CONSTRAINT

In this section we discuss the upper bound for $\sin^2 2\theta_{ee}$ which can be obtained from the data of solar neutrino experiments [32, 56–66] and from the data of the KamLAND very-long-baseline reactor antineutrino experiment [67], which are sensitive to oscillations generated by the small squared-mass difference Δm_{21}^2 . Since the event rates measured in these experiments are well described by standard three-neutrino mixing, the data allow us to constrain the corrections due to active-sterile neutrino mixing, which affects the electron neutrino and antineutrino survival probability and generates transitions into sterile neutrinos [23–26, 68, 69]. As explained in the following, the almost degenerate effects in the solar and KamLAND experiments [24–26] of $|U_{e4}|^2$, which determines $\sin^2 2\theta_{ee}$ through Eq. (4), and $|U_{e3}|^2$ can be resolved by using the recent determination of $|U_{e3}|^2$ in the Daya Bay [70] and RENO [71] long-baseline reactor antineutrino experiments.

The effective survival probability of electron neutrinos and antineutrinos in the solar and KamLAND experi-

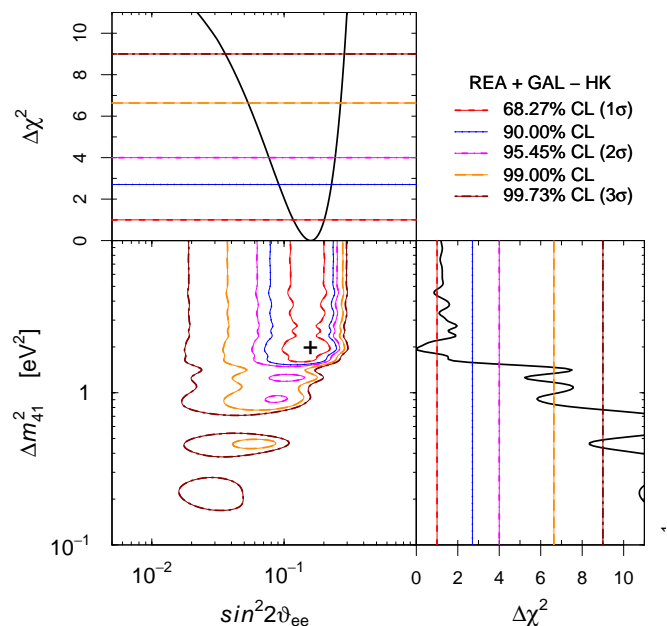


FIG. 7. Allowed regions in the $\sin^2 2\theta_{ee}-\Delta m_{41}^2$ plane and marginal $\Delta\chi^2$'s for $\sin^2 2\theta_{ee}$ and Δm_{41}^2 obtained from the combined fit of Gallium and reactor data in the HF case discussed in Section II. The best-fit point corresponding to χ_{\min}^2 is indicated by a cross.

ments is given by² [72]

$$P_{\nu_e \rightarrow \nu_e}^{\text{SUN}} = P_{\nu_e \rightarrow \nu_e}^{2\nu} \left(1 - \sum_{k=3}^4 |U_{ek}|^2 \right)^2 + \sum_{k=3}^4 |U_{ek}|^4, \quad (18)$$

where $P_{\nu_e \rightarrow \nu_e}^{2\nu}$ is the two-neutrino survival probability generated by Δm_{21}^2 . Considering small values of $|U_{e3}|^2$ and $|U_{e4}|^2$, we have

$$P_{\nu_e \rightarrow \nu_e}^{\text{SUN}} \simeq P_{\nu_e \rightarrow \nu_e}^{2\nu} \left(1 - 2 \sum_{k=3}^4 |U_{ek}|^2 \right). \quad (19)$$

In vacuum the two-neutrino survival probability $P_{\nu_e \rightarrow \nu_e}^{2\nu}$ has the standard two-neutrino form which does not depend on $|U_{e3}|^2$ and $|U_{e4}|^2$. Therefore, in the KamLAND experiment $|U_{e3}|^2$ and $|U_{e4}|^2$ have the same effect of suppressing the electron neutrino and antineutrino survival probability. For solar neutrinos, the main effect of $|U_{e3}|^2$ and $|U_{e4}|^2$ is the same as in the vacuum case, but there are corrections caused by the modifications of $P_{\nu_e \rightarrow \nu_e}^{2\nu}$ due to the decrease of $|U_{e1}|^2 + |U_{e2}|^2 = 1 - (|U_{e3}|^2 + |U_{e4}|^2)$ if $|U_{e3}|^2 \neq 0$ and/or $|U_{e4}|^2 \neq 0$ and to the contribution

² In this discussion we neglect, for simplicity, the matter effects in the Earth which affect the neutrino detection rates in the night, but these effects are taken into account in our calculation.

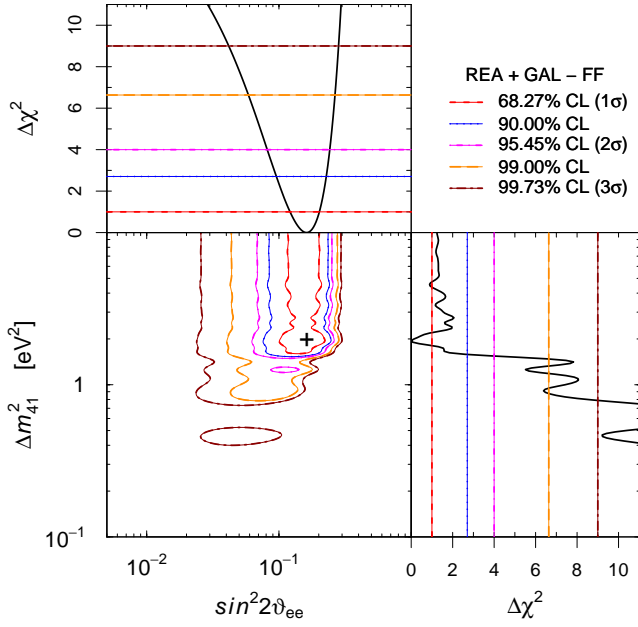


FIG. 8. Allowed regions and marginal $\Delta\chi^2$'s analogous to those in Fig. 7 for the FF case.

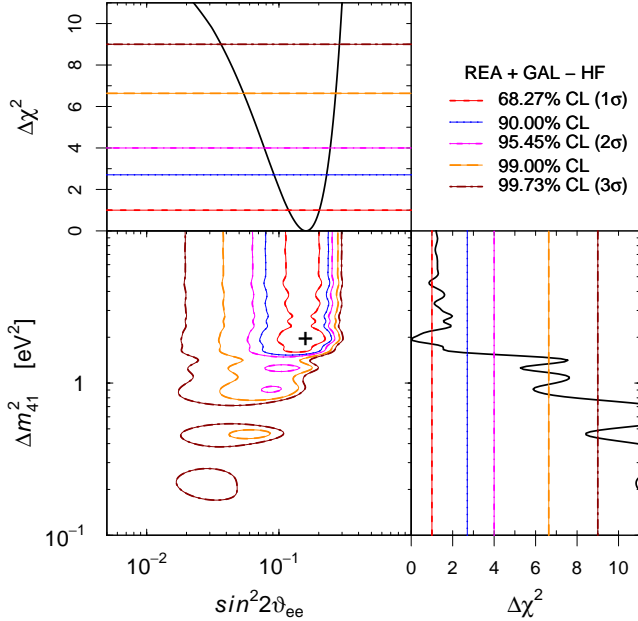


FIG. 9. Allowed regions and marginal $\Delta\chi^2$'s analogous to those in Fig. 7 for the HF case.

of the neutral current potential V_{NC} which is not felt by the sterile neutrino during propagation in matter.

In order to describe this effect, we neglect possible CP-violating phases in the mixing matrix and we parameterize it as (see also [24])

$$U = R_{23}R_{24}R_{34}R_{14}R_{13}R_{12}, \quad (20)$$

where R_{ab} is the real orthogonal matrix ($R_{ab}^T = R_{ab}^{-1}$) which operates a rotation in the a - b plane by an angle ϑ_{ab} :

$$[R^{ab}]_{rs} = \delta_{rs} + (c_{ab} - 1)(\delta_{ra}\delta_{sa} + \delta_{rb}\delta_{sb}) + s_{ab}(\delta_{ra}\delta_{sb} - \delta_{rb}\delta_{sa}), \quad (21)$$

with $c_{ab} \equiv \cos \vartheta_{ab}$ and $s_{ab} \equiv \sin \vartheta_{ab}$. In this parameterization the electron line of the mixing matrix is given by

$$U_{e1} = c_{12}c_{13}c_{14}, \quad U_{e2} = s_{12}c_{13}c_{14}, \quad (22)$$

$$U_{e3} = s_{13}c_{14}, \quad U_{e4} = s_{14}. \quad (23)$$

Hence, this is an extension of the standard three-neutrino mixing parameterization of the electron line (see [1-3]) with the addition of ν_e - ν_4 mixing parameterized by ϑ_{14} . This parameterization is also convenient because

$$\vartheta_{ee} = \vartheta_{14}. \quad (24)$$

Since the sterile line of the mixing matrix is more complicated, it is convenient to write its first two elements as

$$U_{s1} = \cos \varphi_s \cos \chi_s, \quad U_{s2} = \sin \varphi_s \cos \chi_s, \quad (25)$$

with

$$\tan \varphi_s = \frac{Z s_{12} c_{24} + c_{12} s_{24}}{Z c_{12} c_{24} - s_{12} s_{24}}, \quad (26)$$

$$\cos^2 \chi_s = 1 - \sum_{k=3}^4 |U_{sk}|^2 = Z^2 c_{24}^2 + s_{24}^2, \quad (27)$$

$$Z = c_{13}c_{34}s_{14} - s_{13}s_{34}. \quad (28)$$

The adiabatic two-neutrino survival probability $P_{\nu_e \rightarrow \nu_e}^{2\nu}$ is given by [23]

$$P_{\nu_e \rightarrow \nu_e}^{2\nu} = \frac{1}{2} (1 + \cos 2\vartheta_{12} \cos 2\vartheta_{12}^0), \quad (29)$$

where ϑ_{12}^0 is the effective mixing angle at neutrino production, which is given by

$$\vartheta_{12}^0 = \vartheta_{12} + \omega, \quad (30)$$

The mixing angle ω between the vacuum mass basis and the effective mass basis in matter is given by

$$\tan 2\omega = \frac{2EV \sin 2\xi}{\Delta m_{21}^2 - 2EV \cos 2\xi}. \quad (31)$$

Here V is the matter potential given by

$$V^2 = V_{\text{CC}}^2 c_{13}^4 c_{14}^4 + V_{\text{NC}}^2 \cos^4 \chi_s - 2V_{\text{CC}}V_{\text{NC}} \cos 2(\vartheta_{12} - \varphi_s) c_{13}^2 c_{14}^2 \cos^2 \chi_s, \quad (32)$$

where V_{CC} and V_{NC} are the standard charged-current and neutral-current matter potentials. The angle ξ is given by

$$\tan 2\xi = \frac{V_{\text{CC}} \sin 2\vartheta_{12} c_{13}^2 c_{14}^2 - V_{\text{NC}} \sin 2\varphi_s \cos^2 \chi_s}{V_{\text{CC}} \cos 2\vartheta_{12} c_{13}^2 c_{14}^2 - V_{\text{NC}} \cos 2\varphi_s \cos^2 \chi_s}. \quad (33)$$

Therefore, for $s_{14} \ll 1$ the contributions of $|U_{e3}|^2 \simeq s_{13}^2$ and $|U_{e4}|^2 = s_{14}^2$ to the matter effects are almost degenerate. There is only a small difference of their contributions due to Z in Eq. (28).

In solar neutrino measurements the degeneracy of the effects of $|U_{e3}|^2$ and $|U_{e4}|^2$ is also slightly broken by the SNO neutral current measurement, which is sensitive to the total probability of ν_e transitions into active neutrinos, which by unitarity is given by $1 - P_{\nu_e \rightarrow \nu_s}^{\text{SUN}}$, with

$$P_{\nu_e \rightarrow \nu_s}^{\text{SUN}} = P_{\nu_e \rightarrow \nu_s}^{2\nu} c_{13}^2 c_{14}^2 \cos^2 \chi_s + \sum_{k=3}^4 |U_{ek}|^2 |U_{sk}|^2. \quad (34)$$

Here, the adiabatic two-neutrino transition probability $P_{\nu_e \rightarrow \nu_s}^{2\nu}$ is given by³ [23]

$$P_{\nu_e \rightarrow \nu_s}^{2\nu} = \frac{1}{2} (1 + \cos 2\varphi_s \cos 2\vartheta_{12}^0). \quad (35)$$

The degeneracy of $|U_{e3}|^2$ and $|U_{e4}|^2$ is broken by their different effects in φ_s , χ_s and in the last term of Eq. (34).

Luckily, the recent determination of the value of ϑ_{13} in the Daya Bay [70] and RENO [71] experiment allow us to obtain information on the value of $\vartheta_{ee} = \vartheta_{14}$ without much uncertainty due to ϑ_{13} . In the 3+1 mixing scheme under consideration the effective long-baseline $\bar{\nu}_e$ survival probability in the Daya Bay and RENO far detectors is given by [73]

$$P_{\bar{\nu}_e \rightarrow \bar{\nu}_e}^{\text{LBL-F}} = 1 - c_{14}^4 \sin^2 2\vartheta_{13} \sin^2 \left(\frac{\Delta m_{31}^2 L}{4E} \right) - \frac{1}{2} \sin^2 2\vartheta_{14}, \quad (36)$$

since the oscillations due to $\Delta m_{41}^2 \gg \Delta m_{31}^2$ are averaged and the oscillations due to $\Delta m_{21}^2 \ll \Delta m_{31}^2$ are negligibly small. This survival probability depends on ϑ_{14} , but the Daya Bay and RENO collaborations measured the ratio of the probability (36) in the far detectors and the probability (36) with $\Delta m_{31}^2 L / 4E \ll 1$ in the near detectors,

$$P_{\bar{\nu}_e \rightarrow \bar{\nu}_e}^{\text{LBL-N}} = 1 - \frac{1}{2} \sin^2 2\vartheta_{14}. \quad (37)$$

Since the contribution of small values of ϑ_{14} to the measured ratio is of order ϑ_{14}^4 [74], in practice the value of ϑ_{13} determined by the Daya Bay and RENO collaborations with a three-neutrino mixing survival probability is accurate also in the 3+1 scheme under consideration. Nevertheless, since we have the possibility, in our analysis we took into account the exact ratio of the far and near survival probabilities (36) and (37) by including the least-squares function χ_{LBL}^2 of the far/near relative measurements of Daya Bay and RENO in the total solar and reactor least-squares function

$$\chi^2 = \chi_{\text{SOL}}^2 + \chi_{\text{KL}}^2 + \chi_{\text{LBL}}^2. \quad (38)$$

³ One can check that in the limit of two-neutrino ν_e - ν_s mixing the unitarity relation $P_{\nu_e \rightarrow \nu_e}^{2\nu} + P_{\nu_e \rightarrow \nu_s}^{2\nu} = 1$ is satisfied. In this case, $c_{13} = c_{14} = s_{24} = \cos \chi_s = 1$ and $\varphi_s = \vartheta_{12} + \pi/2$.

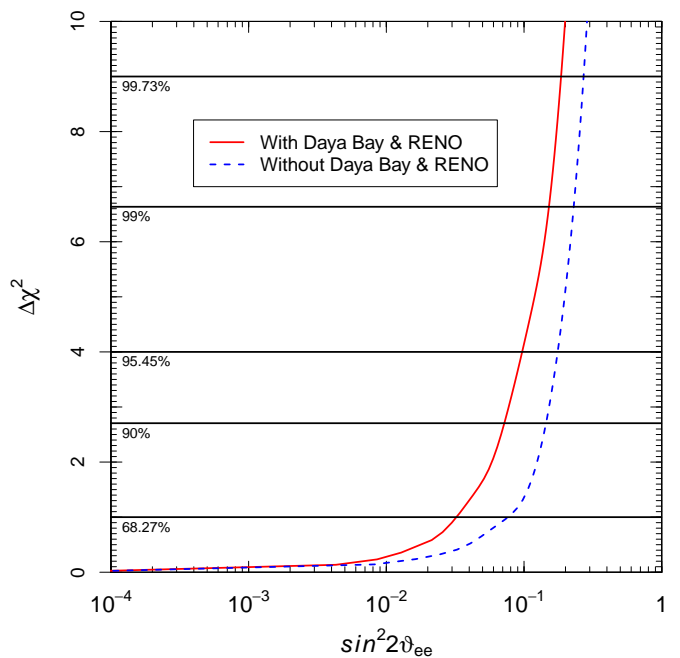


FIG. 10. Marginalized $\Delta\chi^2 = \chi^2 - \chi_{\text{min}}^2$ as a function of $\sin^2 2\vartheta_{ee}$ obtained from the fit of solar and KamLAND data with and without Daya Bay and RENO data.

For the calculation of the solar least-squares function χ_{SOL}^2 , we considered the radiochemical ^{37}Cl [56] and ^{71}Ga [32, 57] experiments, the day and night energy spectra of all four phases of Super-Kamiokande [58–61], the day and night energy spectra of the SNO D₂O phase [62], the charged-current and neutral-current rates of the SNO salt [63] and NCD [64] phases, and the rates of low energy ^7Be [65] and pep [66] solar neutrinos from the Borexino experiment. We did not use the SNO data obtained with the low energy threshold analysis [75] and those obtained with the combined analysis [76] because both analyses assumed a three-parameter polynomial survival probability which is not appropriate for the sterile neutrino analysis. The solar neutrino fluxes are taken from the BP2004 [77] standard solar model, except for the normalization of the solar ^8B neutrino flux, which is considered as a free parameter determined by the minimization of χ^2 (as usual, because of its large theoretical uncertainties).

The KamLAND least-squares function χ_{KL}^2 has been calculated using the energy spectrum reported in [67] with a total exposure of 3.49×10^{32} target-proton-year.

In our analysis, we used the ν_e survival probability (18) and the $\nu_e \rightarrow \nu_s$ transition probability (34) taking into account as parameters the squared-mass difference Δm_{21}^2 and the five relevant mixing angles ϑ_{12} , ϑ_{13} , ϑ_{14} , ϑ_{24} , ϑ_{34} (solar and KamLAND oscillations are independent from ϑ_{23} , because ν_μ and ν_τ are indistinguishable; see [1]). The six-dimensional parameter space is explored with a Markov Chain Monte Carlo sampling in order to minimize the total χ^2 in Eq. (38).

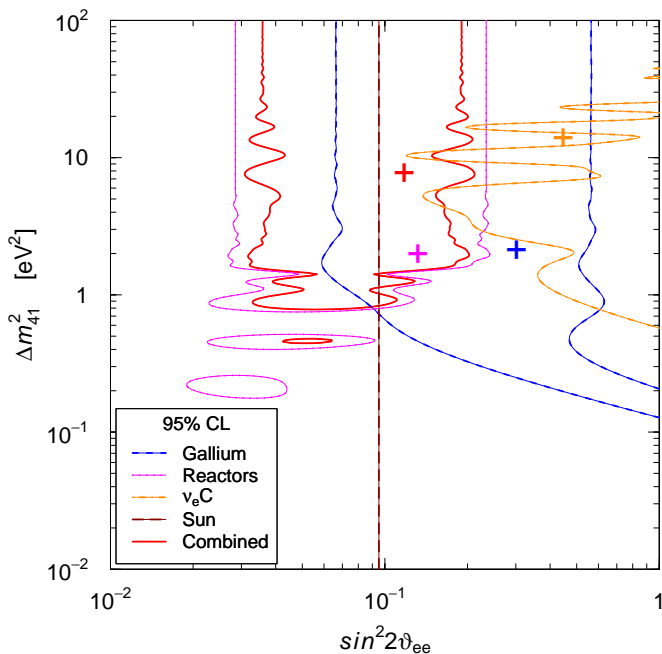


FIG. 11. Allowed 95% CL regions in the $\sin^2 2\vartheta_{ee}-\Delta m_{41}^2$ plane obtained from the separate fits of Gallium, reactor, solar and $\nu_e C$ scattering data and from the combined fit of all data. The best-fit points corresponding to χ_{\min}^2 are indicated by crosses.

Since the best fit is obtained for $\vartheta_{14} = 0$, the marginalized $\Delta\chi^2 = \chi^2 - \chi_{\min}^2$ shown in Fig. 10 give stringent constraints on the value of $\sin^2 2\vartheta_{ee} = \sin^2 2\vartheta_{14}$. In Fig. 10 we have plotted the $\Delta\chi^2$ obtained with and without including the Daya Bay and RENO data. One can see that these data are useful in order to tighten the upper bound on $\sin^2 2\vartheta_{ee}$.

V. GLOBAL FIT

In this section we present the results of the global fit of electron neutrino and antineutrino disappearance data, which includes the Gallium and reactor data discussed respectively in Sections II and III, the solar neutrino constraint discussed in Section IV, and the KARMEN [78, 79] and LSND [80] $\nu_e + {}^{12}\text{C} \rightarrow {}^{12}\text{N}_{\text{g.s.}} + e^-$ scattering data [27], with the method discussed in Ref. [28].

Figure 11 shows a comparison of the allowed 95% CL regions in the $\sin^2 2\vartheta_{ee}-\Delta m_{41}^2$ plane obtained from the separate fits of Gallium, reactor, solar and $\nu_e C$ scattering data and from the combined fit of all data. One can see that the separate allowed regions overlap in a band delimited by $\Delta m_{41}^2 \gtrsim 1 \text{ eV}^2$ and $0.07 \lesssim \sin^2 2\vartheta_{ee} \lesssim 0.09$, which is included in the globally allowed 95% CL region. Figure 12 shows the globally allowed regions in the $\sin^2 2\vartheta_{ee}-\Delta m_{41}^2$ plane and the marginal $\Delta\chi^2$'s for the two oscillation parameters. The best-fit point is at a

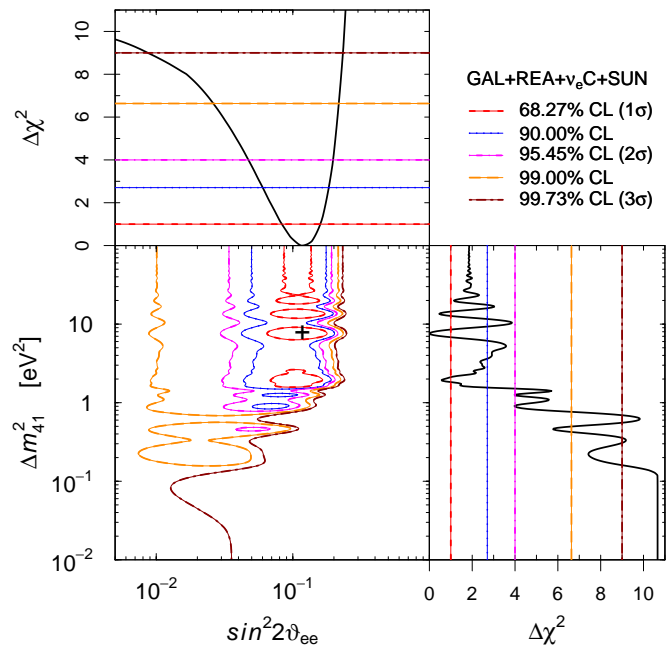


FIG. 12. Allowed regions in the $\sin^2 2\vartheta_{ee}-\Delta m_{41}^2$ plane and marginal $\Delta\chi^2$'s for $\sin^2 2\vartheta_{ee}$ and Δm_{41}^2 obtained from the global fit of ν_e and $\bar{\nu}_e$ data. The best-fit point corresponding to χ_{\min}^2 is indicated by a cross.

relatively large value of Δm_{41}^2 ,

$$(\Delta m_{41}^2)_{\text{bf}} = 7.6 \text{ eV}^2, \quad (\sin^2 2\vartheta_{ee})_{\text{bf}} = 0.12, \quad (39)$$

with $\chi_{\min}^2/\text{NDF} = 45.5/51$, corresponding to a 69% goodness-of-fit. However, there is a region allowed at 1σ around $\Delta m_{41}^2 \simeq 2 \text{ eV}^2$ and $\sin^2 2\vartheta_{ee} \simeq 0.1$. The slight preference of the global fit for $\Delta m_{41}^2 \simeq 7.6 \text{ eV}^2$ with respect to $\Delta m_{41}^2 \simeq 2 \text{ eV}^2$ (see the marginal $\Delta\chi^2$ for Δm_{41}^2 in Fig. 12), which is preferred by Gallium and reactor data (see Tabs. V and VI and Figs. 2–4, 6 and 7–9), is due to the $\nu_e C$ scattering data, which prefer larger values of Δm_{41}^2 (see the discussion in Ref. [28]).

Comparing the minimum of the χ^2 of the global fit with the sum of the minima of the χ^2 of the separate fits of Gallium, reactor, solar and $\nu_e C$ scattering data, we obtained $\Delta\chi_{\text{PG}}^2 = 11.5$, with 5 degrees of freedom, which gives a parameter goodness-of-fit of 4%. Therefore, the compatibility of the four data sets is acceptable.

The results of the global fit, as well as the results of the fits of Gallium and reactor data, lead to lower limits for Δm_{41}^2 , but there is no upper limit for Δm_{41}^2 in Figs. 2–4, 6, 7–9 and 12. Hence, one can ask if there are other measurements which constrain large values of Δm_{41}^2 . The answer is positive and comes from the measurements of the effects of heavy neutrino masses on electron spectrum in β -decay far from the end-point, from the results of neutrinoless double- β decay experiments for Majorana neutrinos, and from cosmological measurements. In this

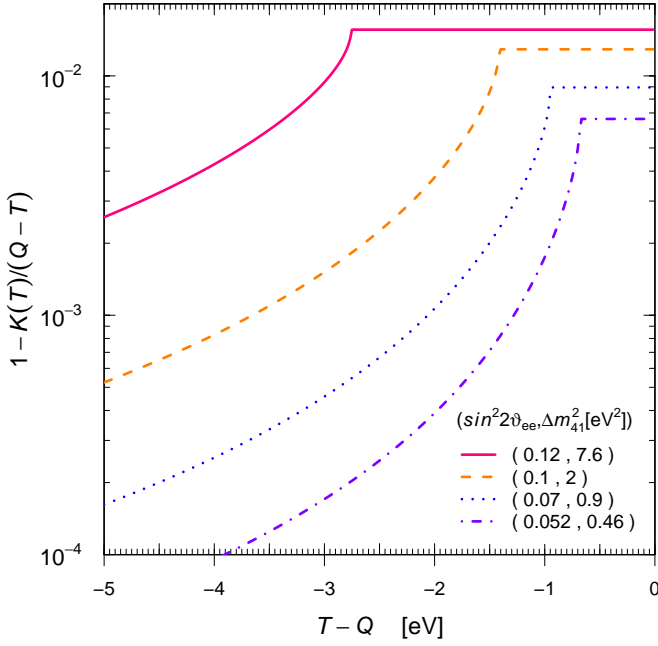


FIG. 13. Relative deviation of the Kurie plot in β -decay for some points in the allowed regions of Fig. 12.

discussion we consider the mass hierarchy

$$m_4 \gg m_1, m_2, m_3, \quad (40)$$

which implies

$$m_4 \simeq \sqrt{\Delta m_{41}^2}. \quad (41)$$

Let us consider first β -decay experiments. The ratio of the Kurie function $K(T)$ in β -decay for the case of a heavy neutrino ν_4 and that corresponding to massless neutrinos is given by [28]

$$\left(\frac{K(T)}{Q-T}\right)^2 = 1 - |U_{e4}|^2 + |U_{e4}|^2 \sqrt{1 - \frac{m_4^2}{(Q-T)^2}} \theta(Q - T - m_4), \quad (42)$$

where T is the kinetic energy of the electron, $Q = 18.574$ keV is the Q -value of the decay, θ is the Heaviside step function, and we have neglected the contribution of the three light neutrinos ν_1, ν_2, ν_3 . Figure 13 shows the relative deviation of the Kurie plot with respect to the massless case for some points in the allowed regions of Fig. 12. One can see that in order to see the effect of m_4 , beta-decay experiments must have a sensitivity to the relative deviation of the Kurie plot of the order of a percent or better for $T \gtrsim Q - m_4$.

In 2001 the Genoa ^{187}Re beta-decay experiment [29] searched for deviation of the electron spectrum due to a heavy neutrino with a mass from 50 to 1000 eV. From

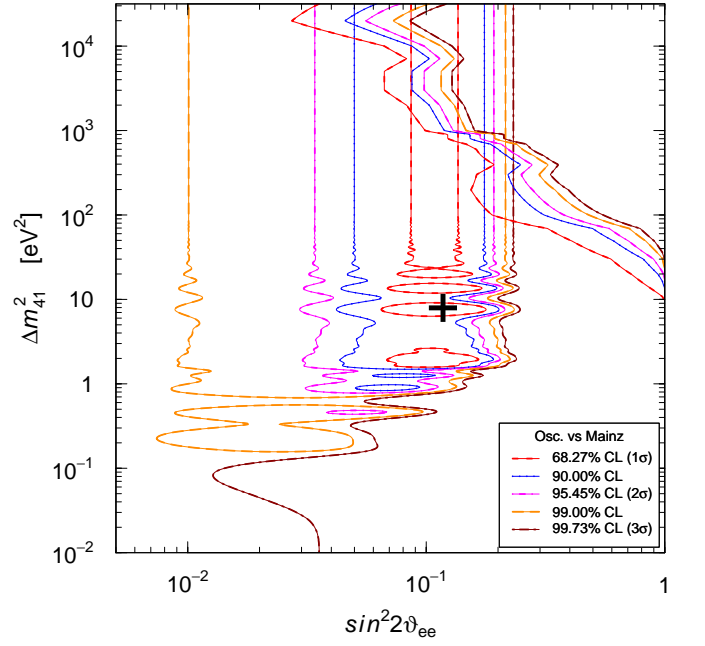


FIG. 14. Comparison of the Mainz β -decay bound (curves in the top-right part of the figure) with the allowed regions in the $\sin^2 2\vartheta_{ee} - \Delta m_{41}^2$ plane obtained from the global fit of ν_e disappearance data (same as in Fig. 12).

Fig. 3 of Ref. [29] one can see that the 95% CL upper bound for m_4 is about 300 eV if $\sin^2 2\vartheta_{ee} \simeq 0.1$, which implies a very large upper limit on Δm_{41}^2 of about 10^5 eV 2 .

Very recently, the Mainz collaboration released new data obtained with the phase II of the Mainz Neutrino Mass Experiment [16] which constrain the value of $\sin^2 \vartheta_{ee}$ for m_4^2 between about 10 and 3×10^4 eV 2 . Figure 14 shows the constraints in the $\sin^2 2\vartheta_{ee} - \Delta m_{41}^2$ plane that we obtained with a χ^2 analysis of the Mainz data in [16]. From the comparison with the allowed regions obtained from the global fit of ν_e disappearance data shown in Fig. 14 one can see that the Mainz data constrain Δm_{41}^2 to be smaller than about 10^4 eV 2 at about 90% CL. This is confirmed by the results of the combined fit shown in Fig. 15.

The KATRIN experiment (see [81]), which will start in 2015 [82], may be able to improve dramatically the upper limits on m_4 and maybe see its effects on the electron spectrum [83].

The heavy neutrino mass m_4 has also an effect in neutrinoless double- β decay (see [84–87]), if massive neutrinos are Majorana particles (see [1–3]). Considering Eq. (41), the contribution of the heavy neutrino mass m_4 to the effective Majorana mass

$$m_{\beta\beta} = \left| \sum_k U_{ek}^2 m_k \right| \quad (43)$$

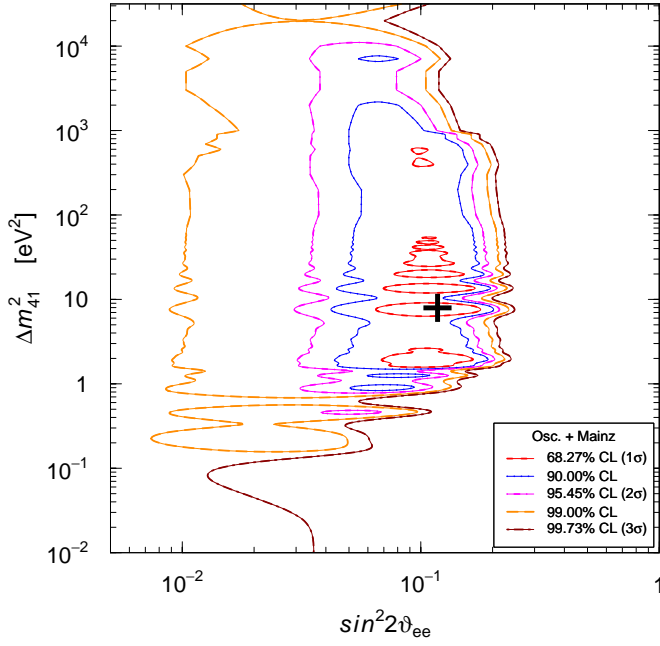


FIG. 15. Allowed regions in the $\sin^2 2\theta_{ee} - \Delta m_{41}^2$ plane obtained from the combined fit of ν_e disappearance and Mainz β -decay data.

is given by

$$m_{\beta\beta}^{(4)} \simeq |U_{e4}|^2 \sqrt{\Delta m_{41}^2}. \quad (44)$$

Figure 16 shows the marginal $\Delta\chi^2 = \chi^2 - \chi_{\min}^2$ as a function of $m_{\beta\beta}^{(4)}$ obtained from the global fit. One can see that $m_{\beta\beta}^{(4)}$ is bounded from below and it is likely to be larger than about 10^{-2} eV, a value which may be reached in the next generation of neutrinoless double- β decay experiment (see [87, 88]). Of course, if the three light neutrinos ν_1, ν_2, ν_3 are quasi-degenerate at a mass scale larger than about 10^{-2} eV the contribution of $m_{\beta\beta}^{(4)}$ can cancel with that of the three light neutrinos. Such an unfortunate cancellation can also happen if the masses of the three light neutrinos follow an inverted hierarchy [89, 90], since in that case their contribution to the effective Majorana mass is [85]

$$1.4 \times 10^{-2} \lesssim m_{\beta\beta}^{(\text{light})} \lesssim 5.0 \times 10^{-2} \text{ eV} \quad (\text{IH} - 95\% \text{ CL}). \quad (45)$$

On the other hand, no cancellation is possible in the case of a normal hierarchy, for which [85]

$$m_{\beta\beta}^{(\text{light})} \lesssim 4.5 \times 10^{-3} \text{ eV} \quad (\text{NH} - 95\% \text{ CL}), \quad (46)$$

and the contribution of $m_{\beta\beta}^{(4)}$ is dominant if it is larger than about 10^{-2} eV. Figure 17 shows the allowed values of $m_{\beta\beta}$ as functions of the lightest neutrino mass in the two 3+1 schemes with a normal (left) and inverted (right)

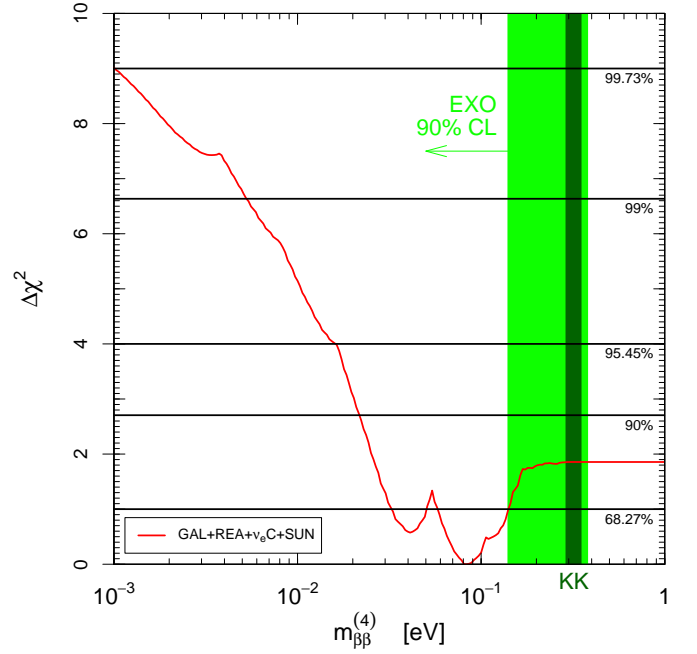


FIG. 16. Marginal $\Delta\chi^2 = \chi^2 - \chi_{\min}^2$ as a function of $m_{\beta\beta}^{(4)}$ obtained from the global fit. The vertical green band represents the currently most stringent 90% CL upper bound for $m_{\beta\beta}^{(4)}$ in the no-cancellation case (47) obtained from the 90% CL EXO bound on $m_{\beta\beta}$ taking into account nuclear matrix element uncertainties [17]. The vertical dark-green band corresponds to the 1σ Klapdor-Kleingrothaus et al. range of $m_{\beta\beta}$ [18].

mass spectra of the three light neutrinos. We have drawn also the curves which delimit the three-neutrino mixing allowed regions [85]. One can see that practically the situation is reversed with respect to the three-neutrino mixing case (see also the discussion in [87]), in which $m_{\beta\beta}$ is predicted to be large in the inverted spectrum and can vanish in the normal spectrum. In the 3+1 case $m_{\beta\beta}$ can have any value in the inverted spectrum, whereas in the normal spectrum it is likely to be large if the three light neutrino masses are hierarchical, i.e. if $m_1 \ll m_2 \ll m_3$.

Let us consider the “no-cancellation” case, in which

$$m_{\beta\beta} \geq m_{\beta\beta}^{(4)} \quad (\text{no-cancellation}). \quad (47)$$

In this case, as shown in Fig. 16, large values of $m_{\beta\beta}^{(4)}$ are excluded by the currently most stringent upper bound for $m_{\beta\beta}$ obtained in the EXO experiment [17] (the vertical green band in Fig. 16 is the 90% CL EXO bound taking into account nuclear matrix element uncertainties). This limit implies the upper bound on $\Delta m_{41}^2 \simeq (m_{\beta\beta}^{(4)} / |U_{e4}|^2)^2$ as a function of $\sin^2 2\theta_{ee}$ shown in Fig. 18. One can see that parts of the high- Δm_{41}^2 regions allowed by the global fit are disfavored by the EXO bound. However, the large nuclear matrix element uncertainties do not allow to establish a precise bound. From Fig. 18 one can also see that the putative Klapdor-Kleingrothaus et

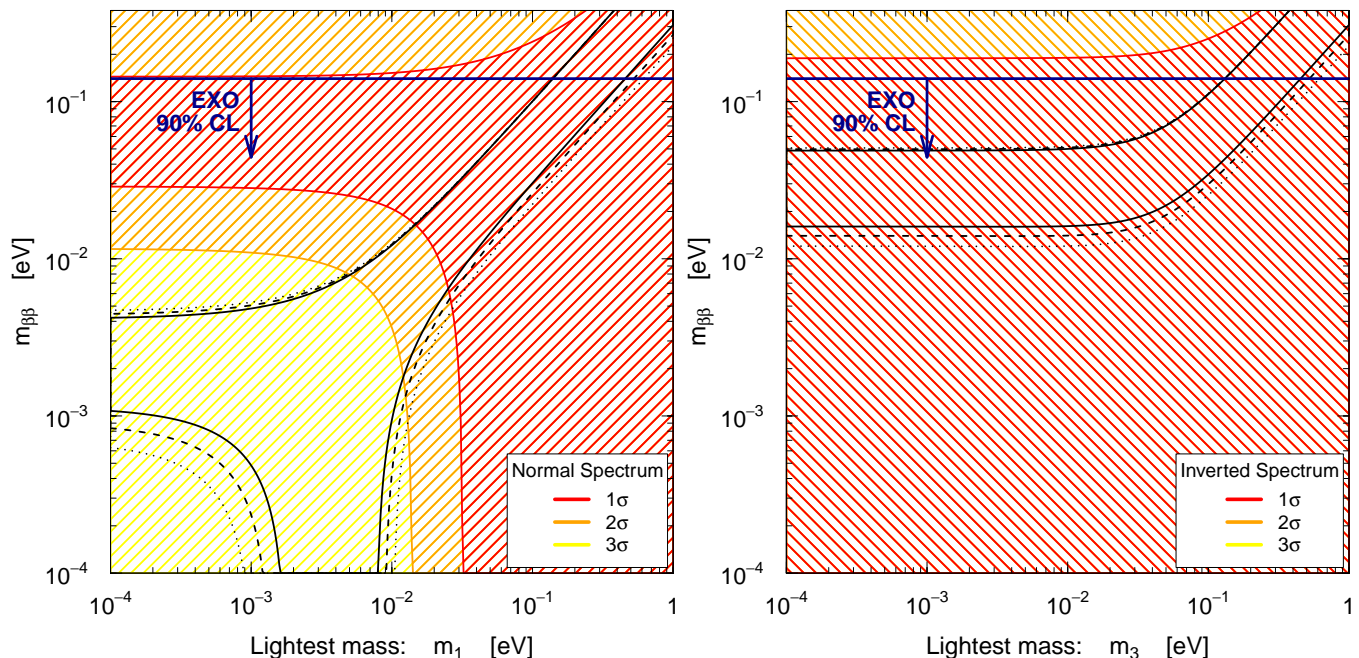


FIG. 17. Allowed ranges of the effective Majorana mass $|m_{\beta\beta}|$ as a function of the lightest neutrino mass in the two 3+1 schemes with a normal (left) and inverted (right) mass spectra of the three light neutrinos ν_1, ν_2, ν_3 . The black lines delimit the three-neutrino mixing allowed regions at 1σ (solid), 2σ (dashed), 3σ (dotted) [85].

al. 1σ range of $m_{\beta\beta}$ [18] implies a rather large value of Δm_{41}^2 , around $100 - 200 \text{ eV}^2$. In this case the oscillation length is very short, of the order of 1 cm for neutrinos with energy of the order of 1 MeV, as reactor neutrinos and neutrinos emitted by radioactive sources. Hence it will be practically impossible to observe a variation of the event rate characteristic of oscillations in future very short-baseline reactor neutrino experiments [91, 92] and radioactive source experiments [93–96] (see also [15, 97]).

Finally, considering cosmological measurements one must say that they are a powerful probe of the number of neutrinos and of neutrino masses at the eV scale (see [15, 98, 99]), but the analysis requires many assumptions on the cosmological model and its details. A comparison of the results of the fit of short-baseline oscillation data is beyond the scope of this paper. We can only say that the analysis of cosmological data in the framework of the standard ΛCDM [48, 100–105] allow the existence of a sterile neutrino thermalized in the early Universe, but restricts its mass to be less than about 1 eV (a possible suppression of the sterile neutrino thermalization with a large lepton asymmetry has been discussed recently in [106, 107]). If this constraint is correct, the upper bound on Δm_{41}^2 is about 1 eV^2 , which is much more restrictive than those of β decay in Fig. 14 and neutrinoless double- β decay in Fig. 18.

VI. CONCLUSIONS

In this paper we presented a complete update of the analysis of ν_e and $\bar{\nu}_e$ disappearance experiments in terms of neutrino oscillations in the framework of 3+1 neutrino mixing. We have shown that the Gallium anomaly, the reactor anomaly, solar neutrino data and $\nu_e C$ scattering data are compatible with short-baseline oscillations with an amplitude $\sin^2 2\vartheta_{ee}$ between about 0.03 and 0.2 and a squared-mass difference Δm_{41}^2 larger than about 0.5 eV^2 at 95% CL. Assuming the mass hierarchy in Eq. (40), we have shown that the heavy neutrino mass m_4 is observable in β -decay experiments and neutrinoless double- β decay experiments. The very recent Mainz β -decay data [16] constrain Δm_{41}^2 to be smaller than about 10^4 eV^2 at 95% CL. For Majorana neutrinos, the recent EXO limit on the effective Majorana mass in neutrinoless double- β decay [17] give a more stringent constraint which can vary between about 10^2 and 10^3 eV^2 depending on the nuclear matrix element uncertainties if there are no cancellations between the contribution of ν_4 and that of the three light neutrinos. We think that our results are interesting for the many projects which will search in the next years effects of light sterile neutrinos with electron neutrino and antineutrino radioactive sources (see [15, 108, 109]), reactor electron antineutrinos (see [15, 110]) and accelerator electron neutrinos [111–113].

Acknowledgments

The work of Y.F. Li is supported in part by the National Natural Science Foundation of China under grant

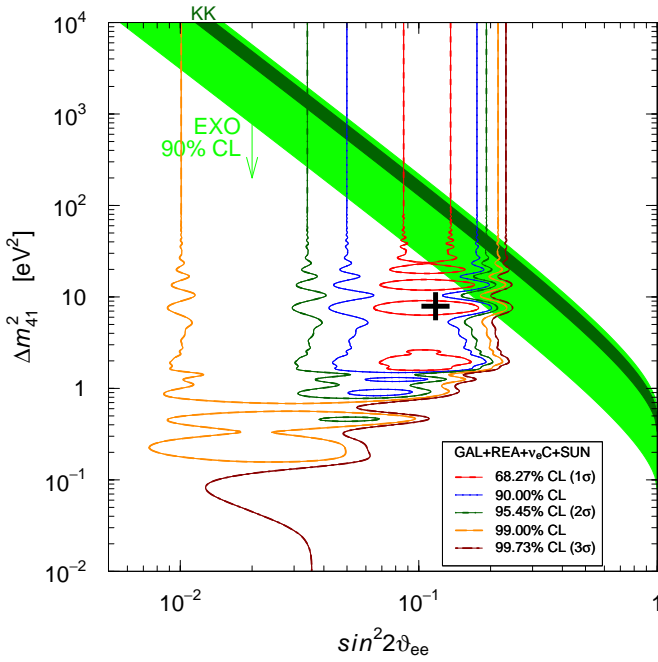


FIG. 18. Comparison of the allowed regions in the $\sin^2 2\theta_{ee}-\Delta m_{41}^2$ plane obtained from the global fit of ν_e disappearance data (same as in Fig. 12) and the bound in the no-cancellation case (47) corresponding to the 90% CL upper bound for $m_{\beta\beta}$ obtained in the EXO experiment taking into account nuclear matrix element uncertainties [17] (green band). The dark-green band corresponds to the 1σ Klapdor-Kleingrothaus et al. range of $m_{\beta\beta}$ [18].

No. 11135009. The work of H.W. Long is supported in part by the National Natural Science Foundation of China under grant No. 11265006.

-
- [1] C. Giunti and C. W. Kim, *Fundamentals of Neutrino Physics and Astrophysics* (Oxford University Press, Oxford, UK, 2007), ISBN 978-0-19-850871-7.
- [2] S. Bilenky, *Introduction to the physics of massive and mixed neutrinos* (Springer, 2010), Lecture Notes in Physics, Volume 817; ISBN 978-3-642-14042-6.
- [3] Z.-z. Xing and S. Zhou, *Neutrinos in particle physics, astronomy and cosmology* (Zhejiang University Press, 2011), ISBN 978-7-308-08024-8.
- [4] M. Laveder, Nucl. Phys. Proc. Suppl. **168**, 344 (2007), Workshop on Neutrino Oscillation Physics (NOW 2006), Otranto, Lecce, Italy, 9-16 Sep 2006.
- [5] C. Giunti and M. Laveder, Mod. Phys. Lett. **A22**, 2499 (2007), hep-ph/0610352.
- [6] C. Giunti and M. Laveder, Phys. Rev. **C83**, 065504 (2011), arXiv:1006.3244.
- [7] T. A. Mueller et al., Phys. Rev. **C83**, 054615 (2011), arXiv:1101.2663.
- [8] P. Huber, Phys. Rev. **C84**, 024617 (2011), arXiv:1106.0687.
- [9] G. Mention et al., Phys. Rev. **D83**, 073006 (2011), arXiv:1101.2755.
- [10] LSND, A. Aguilar et al., Phys. Rev. **D64**, 112007 (2001), hep-ex/0104049.
- [11] MiniBooNE, A. A. Aguilar-Arevalo et al., (2012), arXiv:1207.4809.
- [12] C. Giunti, M. Laveder, Y. Li, Q. Liu, and H. Long, (2012), In Preparation.
- [13] ALEPH, DELPHI, L3, OPAL, SLD, LEP Electroweak Working Group, SLD Electroweak Group, SLD Heavy Flavour Group, S. Schael et al., Phys. Rept. **427**, 257 (2006), hep-ex/0509008.
- [14] D. Frekers et al., Phys. Lett. **B706**, 134 (2011).
- [15] K. N. Abazajian et al., (2012), arXiv:1204.5379.
- [16] C. Kraus, A. Singer, K. Valerius, and C. Weinheimer, (2012), arXiv:1210.4194.
- [17] EXO Collaboration, M. Auger et al., (2012), arXiv:1205.5608.
- [18] H. V. Klapdor-Kleingrothaus and I. V. Krivosheina, Mod. Phys. Lett. **A21**, 1547 (2006).
- [19] S. M. Bilenky, C. Giunti, and W. Grimus, Prog. Part. Nucl. Phys. **43**, 1 (1999), hep-ph/9812360.
- [20] M. Maltoni, T. Schwetz, M. Tortola, and J. Valle, New J. Phys. **6**, 122 (2004), hep-ph/0405172.
- [21] A. Strumia and F. Vissani, (2006), hep-ph/0606054.
- [22] M. C. Gonzalez-Garcia and M. Maltoni, Phys. Rept. **460**, 1 (2008), arXiv:0704.1800.
- [23] C. Giunti and Y. Li, Phys. Rev. **D80**, 113007 (2009), arXiv:0910.5856.
- [24] A. Palazzo, Phys. Rev. **D83**, 113013 (2011), arXiv:1105.1705.
- [25] A. Palazzo, Phys. Rev. **D85**, 077301 (2012),

- arXiv:1201.4280.
- [26] A. Palazzo, (2012), NOW 2012, Neutrino Oscillation Workshop, 9-16 September 2012, Conca Specchiulla, Otranto, Italy.
- [27] J. Conrad and M. Shaevitz, Phys. Rev. **D85**, 013017 (2012), arXiv:1106.5552.
- [28] C. Giunti and M. Laveder, Phys. Lett. **B706**, 200 (2011), arXiv:1111.1069.
- [29] M. Galeazzi, F. Fontanelli, F. Gatti, and S. Vitale, Phys. Rev. Lett. **86**, 1978 (2001).
- [30] GALLEX, P. Anselmann *et al.*, Phys. Lett. **B342**, 440 (1995).
- [31] GALLEX, W. Hampel *et al.*, Phys. Lett. **B420**, 114 (1998).
- [32] F. Kaether, W. Hampel, G. Heusser, J. Kiko, and T. Kirsten, Phys. Lett. **B685**, 47 (2010), arXiv:1001.2731.
- [33] SAGE, J. N. Abdurashitov *et al.*, Phys. Rev. Lett. **77**, 4708 (1996).
- [34] SAGE, J. N. Abdurashitov *et al.*, Phys. Rev. **C59**, 2246 (1999), hep-ph/9803418.
- [35] J. N. Abdurashitov *et al.*, Phys. Rev. **C73**, 045805 (2006), nucl-ex/0512041.
- [36] SAGE, J. N. Abdurashitov *et al.*, Phys. Rev. **C80**, 015807 (2009), arXiv:0901.2200.
- [37] J. N. Bahcall, Phys. Rev. **C56**, 3391 (1997), hep-ph/9710491.
- [38] D. Krofcheck *et al.*, Phys. Rev. Lett. **55**, 1051 (1985).
- [39] D. Krofcheck, (1987), PhD Thesis, Ohio State University.
- [40] W. C. Haxton, Phys. Lett. **B431**, 110 (1998), nucl-th/9804011.
- [41] J. N. Bahcall, *Neutrino Astrophysics* (Cambridge University Press, 1989).
- [42] Particle Data Group, J. Beringer *et al.*, Phys. Rev. D **86**, 010001 (2012).
- [43] W. Hampel and L. Remsberg, Phys. Rev. **C31**, 666 (1985).
- [44] National Nuclear Data Center, Brookhaven National Laboratory, (2012), <http://www.nndc.bnl.gov/logft/>.
- [45] C. Giunti and M. Laveder, Phys. Rev. **D82**, 113009 (2010), arXiv:1008.4750.
- [46] C. Giunti and M. Laveder, Phys. Rev. **D84**, 073008 (2011), arXiv:1107.1452.
- [47] C. Giunti and M. Laveder, Phys. Rev. **D84**, 093006 (2011), arXiv:1109.4033.
- [48] M. Archidiacono, N. Fornengo, C. Giunti, and A. Melchiorri, Phys. Rev. **D86**, 065028 (2012), arXiv:1207.6515.
- [49] Bugey, B. Achkar *et al.*, Nucl. Phys. **B434**, 503 (1995).
- [50] Bugey, Y. Declais *et al.*, Phys. Lett. **B338**, 383 (1994).
- [51] A. Kuvshinnikov, L. Mikaelyan, S. Nikolaev, M. Skokhvatov, and A. Etenko, JETP Lett. **54**, 253 (1991).
- [52] CalTech-SIN-TUM, G. Zacek *et al.*, Phys. Rev. **D34**, 2621 (1986).
- [53] A. Hoummada, S. Lazrak Mikou, G. Bagieu, J. Cavaignac, and D. Holm Koang, Applied Radiation and Isotopes **46**, 449 (1995).
- [54] Krasnoyarsk, G. S. Vidyakin *et al.*, Sov. Phys. JETP **71**, 424 (1990).
- [55] M. Maltoni and T. Schwetz, Phys. Rev. **D68**, 033020 (2003), hep-ph/0304176.
- [56] Homestake, B. T. Cleveland *et al.*, Astrophys. J. **496**, 505 (1998).
- [57] SAGE, J. N. Abdurashitov *et al.*, J. Exp. Theor. Phys. **95**, 181 (2002), astro-ph/0204245.
- [58] Super-Kamiokande, J. Hosaka *et al.*, Phys. Rev. **D73**, 112001 (2006), hep-ex/0508053.
- [59] Super-Kamiokande, J. Cravens *et al.*, Phys. Rev. **D78**, 032002 (2008), arXiv:0803.4312.
- [60] Super-Kamiokande, K. Abe *et al.*, Phys. Rev. **D83**, 052010 (2011), arXiv:1010.0118.
- [61] Super-Kamiokande, M. Smy, (2012), Neutrino 2012, XXV International Conference on Neutrino Physics and Astrophysics, 3-9 June 2012, Kyoto, Japan.
- [62] SNO, Q. R. Ahmad *et al.*, Phys. Rev. Lett. **89**, 011302 (2002), nucl-ex/0204009.
- [63] SNO, B. Aharmim *et al.*, Phys. Rev. **C72**, 055502 (2005), nucl-ex/0502021.
- [64] SNO, B. Aharmim *et al.*, Phys. Rev. Lett. **101**, 111301 (2008), arXiv:0806.0989.
- [65] Borexino, G. Bellini *et al.*, Phys. Rev. Lett. **107**, 141302 (2011), arXiv:1104.1816.
- [66] Borexino, G. Bellini *et al.*, Phys. Rev. Lett. **108**, 051302 (2012), arXiv:1110.3230.
- [67] KamLAND, A. Gando *et al.*, Phys. Rev. **D83**, 052002 (2011), arXiv:1009.4771.
- [68] D. Dooling, C. Giunti, K. Kang, and C. W. Kim, Phys. Rev. **D61**, 073011 (2000), hep-ph/9908513.
- [69] C. Giunti, M. C. Gonzalez-Garcia, and C. Pena-Garay, Phys. Rev. **D62**, 013005 (2000), hep-ph/0001101.
- [70] Daya Bay, F. P. An *et al.*, Phys. Rev. Lett. **108**, 171803 (2012), arXiv:1203.1669.
- [71] RENO, S.-B. Kim *et al.*, Phys. Rev. Lett. **108**, 191802 (2012), arXiv:1204.0626.
- [72] S. M. Bilenky, C. Giunti, and W. Grimus, Eur. Phys. J. **C1**, 247 (1998), hep-ph/9607372.
- [73] A. de Gouvea and T. Wytock, Phys. Rev. **D79**, 073005 (2009), arXiv:0809.5076.
- [74] C. Giunti and M. Laveder, Phys. Rev. **D85**, 031301 (2012), arXiv:1111.5211.
- [75] SNO, B. Aharmim *et al.*, Phys. Rev. **C81**, 055504 (2010), arXiv:0910.2984.
- [76] SNO, B. Aharmim *et al.*, (2011), arXiv:1109.0763.
- [77] J. N. Bahcall and M. H. Pinsonneault, Phys. Rev. Lett. **92**, 121301 (2004), astro-ph/0402114.
- [78] KARMEN., B. E. Bodmann *et al.*, Phys. Lett. **B332**, 251 (1994).
- [79] KARMEN, B. Armbruster *et al.*, Phys. Rev. **C57**, 3414 (1998), hep-ex/9801007.
- [80] LSND, L. B. Auerbach *et al.*, Phys. Rev. **C64**, 065501 (2001), hep-ex/0105068.
- [81] E. Otten and C. Weinheimer, Rept. Prog. Phys. **71**, 086201 (2008), arXiv:0909.2104.
- [82] KATRIN, J. Wolf, (2012), NPB 2012, International Symposium on Neutrino Physics and Beyond, 23-26 September 2012, Shenzhen, China.
- [83] A. Esmaili and O. L. G. Peres, Phys. Rev. **D85**, 117301 (2012), arXiv:1203.2632.
- [84] J. Gomez-Cadenas, J. Martin-Albo, M. Mezzetto, F. Monrabal, and M. Sorel, Riv. Nuovo Cim. **35**, 29 (2012), arXiv:1109.5515.
- [85] S. M. Bilenky and C. Giunti, Mod. Phys. Lett. **A27**, 1230015 (2012), arXiv:1203.5250.
- [86] J. D. Vergados, H. Ejiri, and F. Simkovic, Rept. Prog. Phys. **75**, 106301 (2012), arXiv:1205.0649.
- [87] W. Rodejohann, J. Phys. **G39**, 124008 (2012),

- arXiv:1206.2560.
- [88] O. Cremonesi, (2012), NOW 2012, Neutrino Oscillation Workshop, 9-16 September 2012, Conca Specchiulla, Otranto, Italy.
- [89] J. Barry, W. Rodejohann, and H. Zhang, JHEP **07**, 091 (2011), arXiv:1105.3911.
- [90] Y. Li and S. Liu, Phys. Lett. **B706**, 406 (2012), arXiv:1110.5795.
- [91] A. P. Serebrov *et al.*, (2012), arXiv:1205.2955.
- [92] A. V. Derbin, A. S. Kayunov, and V. N. Muratova, (2012), arXiv:1204.2449.
- [93] A. Ianni, D. Montanino, and G. Scioscia, Eur. Phys. J. **C8**, 609 (1999), hep-ex/9901012.
- [94] V. N. Gavrin, V. V. Gorbachev, E. P. Veretenkin, and B. T. Cleveland, (2010), arXiv:1006.2103.
- [95] M. Cribier *et al.*, Phys. Rev. Lett. **107**, 201801 (2011), arXiv:1107.2335.
- [96] A. Bungau *et al.*, (2012), arXiv:1205.4419.
- [97] T. Lasserre, (2012), arXiv:1209.5090, Neutrino 2012 Conference, Kyoto, Japan, June 2012.
- [98] Y. Y. Y. Wong, Ann. Rev. Nucl. Part. Sci. **61**, 69 (2011), arXiv:1111.1436.
- [99] G. Steigman, Adv. High Energy Phys. **2012**, 268321 (2012), arXiv:1208.0032.
- [100] B. A. Reid, L. Verde, R. Jimenez, and O. Mena, JCAP **1001**, 003 (2010), arXiv:0910.0008.
- [101] M. C. Gonzalez-Garcia, M. Maltoni, and J. Salvado, JHEP **08**, 117 (2010), arXiv:1006.3795.
- [102] J. Hamann, S. Hannestad, G. G. Raffelt, I. Tamborra, and Y. Y. Wong, Phys. Rev. Lett. **105**, 181301 (2010), arXiv:1006.5276.
- [103] J. Hamann, S. Hannestad, G. G. Raffelt, and Y. Y. Wong, JCAP **1109**, 034 (2011), arXiv:1108.4136.
- [104] M. Archidiacono, E. Calabrese, and A. Melchiorri, Phys. Rev. **D84**, 123008 (2011), arXiv:1109.2767.
- [105] S. Joudaki, K. N. Abazajian, and M. Kaplinghat, Phys. Rev. **D87**, 065003 (2013), arXiv:1208.4354.
- [106] S. Hannestad, I. Tamborra, and T. Tram, JCAP **1207**, 025 (2012), arXiv:1204.5861.
- [107] A. Mirizzi, N. Saviano, G. Miele, and P. D. Serpico, Phys.Rev. **D86**, 053009 (2012), arXiv:1206.1046.
- [108] A. Ianni, (2012), NOW 2012, Neutrino Oscillation Workshop, 9-16 September 2012, Conca Specchiulla, Otranto, Italy.
- [109] J. Link, (2012), NOW 2012, Neutrino Oscillation Workshop, 9-16 September 2012, Conca Specchiulla, Otranto, Italy.
- [110] J. Gaffiot, (2012), NOW 2012, Neutrino Oscillation Workshop, 9-16 September 2012, Conca Specchiulla, Otranto, Italy.
- [111] M. Antonello *et al.*, (2012), arXiv:1203.3432.
- [112] L. Stanco, (2012), NOW 2012, Neutrino Oscillation Workshop, 9-16 September 2012, Conca Specchiulla, Otranto, Italy.
- [113] D. Gibin, (2012), NOW 2012, Neutrino Oscillation Workshop, 9-16 September 2012, Conca Specchiulla, Otranto, Italy.